2013

Finite Element Analysis of Balloon-Expandable Coronary Stent Deployment: Influence of Angioplasty Balloon Configuration

David Martin
Technological University Dublin, david.martin@tudublin.ie

Fergal Boyle
Technological University Dublin, fergal.boyle@tudublin.ie

Finite element analysis of balloon-expandable coronary stent deployment: Influence of angioplasty balloon configuration

David Martin*,† and Fergal Boyle

Department of Mechanical Engineering, Dublin Institute of Technology, Ireland

SUMMARY

Today, the majority of coronary stents are balloon-expandable and are deployed using a balloon-tipped catheter. To improve deliverability, the membrane of the angioplasty balloon is typically folded about the catheter in a pleated configuration. As such, the deployment of the angioplasty balloon is governed by the material properties of the balloon membrane, its folded configuration and its attachment to the catheter. Despite this observation, however, an optimum strategy for modelling the configuration of the angioplasty balloon in finite element studies of coronary stent deployment has not been identified, and idealised models of the angioplasty balloon are commonly employed in the literature. These idealised models often neglect complex geometrical features, such as the folded configuration of the balloon membrane and its attachment to the catheter, which may have a significant influence on the deployment of a stent. In this study, three increasingly sophisticated models of a typical semi-compliant angioplasty balloon were employed to determine the influence of angioplasty balloon configuration on the deployment of a stent. The results of this study indicate that angioplasty balloon configuration has a significant influence on both the transient behaviour of the stent and its impact on the mechanical environment of the coronary artery. Copyright © 2013 John Wiley & Sons, Ltd.

1. INTRODUCTION

Coronary heart disease, which refers to the failure of the coronary circulation to provide an adequate supply of oxygenated blood to the heart, is currently one of the most common causes of mortality in the developed world [1]. Over the past two decades, however, percutaneous transluminal coronary angioplasty (PTCA) with either bare-metal or drug-eluting balloon-expandable coronary stent deployment has emerged as an effective treatment for coronary heart disease. For most patients who suffer from coronary heart disease, treatment with a stent results in favourable clinical results. For a small subset of patients, however, re-narrowing of the treated artery is observed at follow-up [2–6]. This re-narrowing of the treated artery is referred to as in-stent restenosis, which is typically defined as the presence of a $\geq 50\%$ diameter stenosis in the stented segment of the artery at follow-up [7]. In-stent restenosis is primarily attributed to neointimal hyperplasia, which refers to the uncontrolled proliferation and migration of smooth muscle cells and the associated synthesis and deposition of extracellular matrix within the intimal layer of the artery wall [8, 9].

In recent years, a number of factors linked to stent design and deployment have been associated with the development of neointimal hyperplasia following treatment with a stent. Endothelial denudation and arterial injury incurred during stent deployment has been strongly linked to

---

*Correspondence to: David Martin, Department of Mechanical Engineering, Dublin Institute of Technology, Ireland.
†E-mail: david.martin@dit.ie

neointimal hyperplasia at follow-up [10]. Stent-induced disruption to local vessel hemodynamics has also been associated with dysfunction of the vascular endothelium and subsequent neointimal hyperplasia at follow-up [11]. Finally, the material properties and surface roughness of the stent have been found to influence the severity of the inflammatory response in the artery wall following stent deployment [12]. As these factors are strongly linked to the design of the stent, research in this area is currently centred on the optimisation of stent performance through the identification of high-strength stent materials, improved stent platforms, potent anti-proliferative and anti-inflammatory stent coatings, biocompatible and bioabsorbable carrier materials and novel means of drug-delivery [13].

Because of the difficulty and expense involved in the evaluation of stent performance, numerical methods of analysis have emerged in recent years as powerful investigative tools for stent design and optimisation. To date, a significant number of studies have employed numerical methods of analysis to investigate various aspects of stent performance such as stented-artery hemodynamics, mass transport from drug-eluting stents and the degradation of bioabsorbable stents [14–26]. Because of the strong correlation between stent-induced arterial injury and subsequent neointimal hyperplasia, however, the majority of these studies have focused on investigating stent deployment characteristics and the impact of stent deployment on the mechanical environment of the coronary artery [27–50]. These studies are typically conducted using the finite element method and are reviewed in detail elsewhere [51]. The finite element method is a well-established numerical technique that is generally employed to obtain approximate numerical solutions to intractable analytical problems.

Today, the majority of coronary stents are balloon-expandable and are deployed using a balloon-tipped catheter [52]. To improve deliverability, the membrane of the angioplasty balloon is generally folded about the catheter in a pleated configuration. As a result, the deployment of the angioplasty balloon is governed by the material properties of the balloon membrane, its folded configuration and its attachment to the catheter. To date, an optimum strategy for modelling the configuration of the angioplasty balloon in finite element studies of coronary stent deployment has not been identified, and idealised models of the angioplasty balloon are commonly employed in the literature [28, 31, 32, 36, 37, 39, 42, 45, 49]. These idealised models often neglect complex geometrical features, such as the folded configuration of the balloon membrane and its attachment to the catheter. It is possible that these features have a significant influence on both the deployment characteristics of the stent and its impact on the mechanical environment of the coronary artery. Despite this observation, however, the influence of these geometrical features has not been investigated.

In this study, three increasingly sophisticated finite element models of a typical semi-compliant angioplasty balloon were employed to determine the influence of angioplasty balloon configuration on the deployment of a coronary stent. Both the free deployment of the stent and its deployment within an idealised model of a coronary artery was investigated using (a) an idealised non-folded model, (b) an idealised folded model and (c) a state-of-the-art folded model of a semi-compliant angioplasty balloon. By comparing the results from the analyses, the influence of the folded configuration of the balloon membrane and its attachment to the catheter on both the deployment characteristics of the stent and its impact on the mechanical environment of the coronary artery was evaluated. On the basis of the results of this study, optimum strategies for modelling the configuration of the angioplasty balloon in future finite element studies of coronary stent deployment are recommended.

2. MATERIALS AND METHODS

In this study, two sets of finite element analyses were performed using ABAQUS v6.11 (Dassault Systèmes, Simulia Corporation, Providence, RI, USA). In the first set of analyses, three increasingly sophisticated models of a typical semi-compliant angioplasty balloon were employed to investigate the free deployment of a coronary stent. The results from these analyses were compared to determine the influence of the folded configuration of the balloon membrane and its attachment to the catheter on the free deployment characteristics of the stent. In the second set of analyses, the three angioplasty balloon models were employed to investigate the deployment of the same coronary stent within an idealised cylindrical model of a coronary artery. The results from these analyses
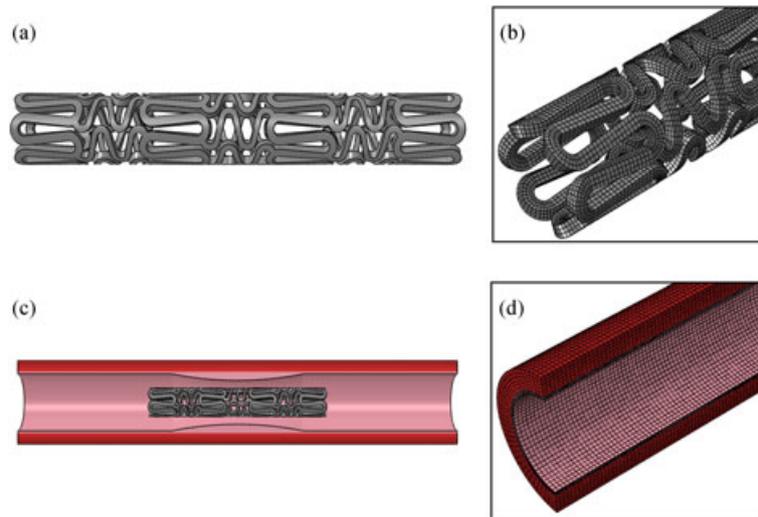
Figure 1. Configuration of (a) the stent, (b) the discretised stent, (c) the atherosclerotic coronary artery and (d) the discretised atherosclerotic coronary artery.

were compared to determine the influence of the folded configuration of the balloon membrane and its attachment to the catheter on both the magnitude and distribution of stent-induced arterial stress.

2.1. Geometry and finite element discretisation

The investigated stent resembles the balloon-expandable BX-Velocity (Cordis, Johnson & Johnson, New Brunswick, NJ, USA) coronary stent, which has a nominal diameter of 3 mm and, as shown in Figure 1, consists of sinusoidal strut segments that are interconnected by flexible link segments in a closed-cell configuration. The stent was initially modelled in a planar configuration in ANSYS v13.0 (ANSYS Inc., Canonsburg, PA, USA) and discretised using 24,750 reduced-integration continuum elements. The cylindrical configuration of the stent was then obtained by transferring nodal coordinates from a Cartesian coordinate system to a cylindrical coordinate system according to a procedure described in the literature [38]. The cylindrical configuration of the stent was then imported into ABAQUS v6.11 for analysis. In its cylindrical configuration, the stent featured internal and external diameters of 1.0 and 1.3 mm, respectively, which resulted in a uniform strut thickness of 0.15 mm.

The BX-Velocity stent is typically deployed using the Raptor (Cordis) PTCA balloon-tipped catheter. The Raptor PTCA balloon-tipped catheter consists of a nylon-based angioplasty balloon that is tri-folded about the tip of a flexible polyethylene-based catheter. The balloon-tipped catheter is then directed through the circulatory system to the occluded segment of a coronary artery over a thin nitinol guide wire. The tri-folded configuration of the Raptor angioplasty balloon was confirmed by De Beule *et al.* from micro-CT images [32]. In its initial configuration, prior to deflation and folding, the Raptor angioplasty balloon has a diameter of approximately 2.85 mm. This value was identified by De Beule *et al.* by extrapolating to zero inflation pressure on the manufacturer's compliance chart [32]. The manufacturer's compliance chart describes the pressure–diameter response of the Raptor angioplasty balloon as derived from *in vitro* experimental measurements.

The first finite element model of the Raptor angioplasty balloon is referred to as balloon A and is shown in its deflated configuration in Figure 2(a). For balloon A, both the tri-folded configuration of the balloon membrane and its attachment to the catheter were neglected. The balloon membrane was assigned a length of 10 mm, a uniform thickness of 0.02 mm and internal and external diameters of 0.5 and 0.75 mm, respectively. The catheter was assigned a length of 12 mm and a diameter of 0.5 mm. The balloon membrane was discretised using 10,000 reduced-integration membrane elements (element type: M3D4R), and the catheter was discretised using 1920 reduced-integration surface elements (element type: SFM3D4R). As balloon A neglects both the folded configuration of the balloon membrane and its attachment to the catheter, it is the simplest angioplasty balloon model
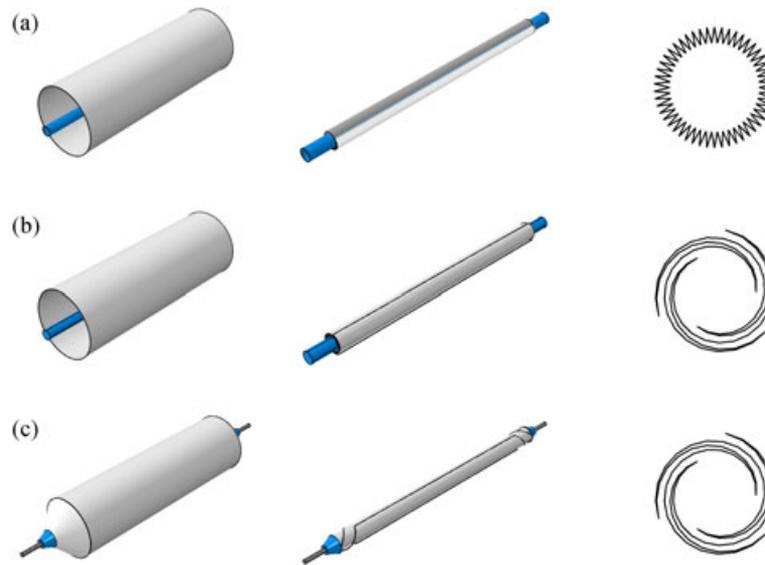
Figure 2. Configuration of (a) balloon A, (b) balloon B and (c) balloon C prior to deflation/folding (left) and following deflation/folding (middle). Cross-sectional profiles of the deflated/folded configuration of the angioplasty balloon models are also shown (right).

considered in this study. Non-folded angioplasty balloon models were first proposed by Brauer *et al*. and have since been employed in a number of studies throughout the literature [53].

The second finite element model of the Raptor angioplasty balloon is referred to as balloon B and is shown in its deflated configuration in Figure 2(b). For balloon B, the tri-folded configuration of the balloon membrane was included, but its attachment to the catheter was neglected. As with balloon A, the balloon membrane was assigned a length of 10 mm, a uniform thickness of 0.02 mm and internal and external diameters of 0.5 and 0.75 mm, respectively. The catheter was assigned a length of 12 mm and a diameter of 0.5 mm. Again, the balloon membrane was discretised using 10,000 reduced-integration membrane elements (element type: M3D4R), and the catheter was discretised using 1920 reduced-integration surface elements (element type: SFM3D4R). As balloon B includes the folded configuration of the balloon membrane, it is a more advanced angioplasty balloon model than balloon A. Folded angioplasty balloon models were first proposed by Laroche *et al*. and have since been employed in a number of studies throughout the literature [54].

The third finite element model of the Raptor angioplasty balloon is referred to as balloon C and is shown in its deflated configuration in Figure 2(c). For balloon C, both the tri-folded configuration of the balloon membrane and its attachment to the catheter were included. The balloon membrane was assigned a length of 12 mm, a uniform thickness of 0.02 mm and internal and external diameters of 0.5 and 0.75 mm, respectively. The catheter and guide wire were assigned lengths of 13 and 15 mm and diameters of 0.5 and 0.2 mm, respectively. The balloon membrane was discretised using 12,462 reduced-integration membrane elements (element type: M3D4R), whereas the catheter and guide wire were discretised using 4800 and 7488 reduced-integration continuum elements (element type: C3D8R), respectively. Nodes located at the extremities of the balloon membrane were then attached to the catheter using tie constraints. As balloon C includes both the folded configuration of the balloon membrane and its attachment to the catheter, it is a more advanced angioplasty balloon model than either balloons A or B. Sophisticated folded angioplasty balloon models were first proposed by Mortier *et al*. and have since been employed in a number of studies throughout the literature [44].

The atherosclerotic coronary artery, shown in Figure 1, was idealised as a straight cylindrical vessel that featured a diffuse atherosclerotic plaque at its mid-section. The artery was assigned a length of 20 mm and internal and external diameters of 2.8 and 3.8 mm, respectively, which resulted in a uniform wall thickness of 0.5 mm. The artery wall was partitioned into three individual layers that represented the intimal, medial and adventitial layers of the coronary artery. The intimal, medial

and adventitial layers were assigned a thickness of 0.145, 0.165 and 0.19 mm, respectively, in accordance with experimental measurements reported in the literature [55]. The diffuse atherosclerotic plaque was modelled as an inner arterial layer that increased in thickness from 0.1 mm at the extremities of the artery to 0.4 mm at its mid-section. This resulted in a maximum wall thickness of 0.9 mm and a maximum reduction in lumen cross-sectional area of approximately 50% at the mid-section of the artery. The artery and plaque were discretised using 88,164 and 58,776 reduced-integration continuum elements (element type: C3D8R), respectively.

2.2. Material properties

The BX-Velocity stent is manufactured from medical-grade 316L stainless-steel and, during its deployment, undergoes significant plastic deformation. In this study, the mechanical behaviour of the stent was described using a rate-independent elastic-plastic material model with isotropic hardening. The properties used to describe the behaviour of the stent were obtained from Poncin *et al.* who performed uniaxial tension tests on fully annealed samples of medical-grade 316L stainless-steel stent tubing [56]. The elastic behaviour of the stent was described using a Young's modulus of 193 GPa and a Poisson's ratio of 0.3. The plastic behaviour of the stent was then described using a multi-linear function that was characterised by a yield stress of 360 MPa and an ultimate tensile stress of 675 MPa.

The balloon membrane, the catheter and the guide wire of the Raptor PTCA balloon-tipped catheter are manufactured from nylon-based, polyethylene-based and nitinol-based materials, respectively. The mechanical behaviour of these components was described using linear elastic material models. The properties used to describe the behaviour of the balloon membrane were obtained from De Beule *et al.* who employed the finite element method to investigate the deployment of balloon-expandable coronary stents [32]. The properties used to describe the behaviour of the catheter and the guide wire were obtained from Mortier *et al.* who employed the finite element method to investigate the deployment of balloon-expandable coronary stents within a coronary bifurcation [43, 44]. The elastic behaviour of the balloon membrane, the catheter and the guide wire was described using Young's moduli of 920 MPa, 1 GPa and 62 GPa and Poisson's ratios of 0.4, 0.4 and 0.3, respectively.

The mechanical behaviour of the individual layers of the coronary artery is highly nonlinear and was described using a third-order Ogden isotropic hyperelastic material model. The properties used to describe the behaviour of the individual layers of the coronary artery were obtained from Holzapfel *et al.* who performed uniaxial tension tests on circumferentially orientated samples of human arterial tissue [55]. The mechanical behaviour of the atherosclerotic plaque is also highly nonlinear and was described using a first-order Ogden isotropic hyperelastic material model. The properties used to describe the behaviour of the atherosclerotic plaque were obtained from Loree *et al.* who performed uniaxial tension tests on samples of human atherosclerotic tissue [57]. The hyperelastic material constants that resulted in the best fit with the experimental data are shown in Table I. These constants were determined using the curve-fitting tool in ABAQUS v6.11. The accuracy of the hyperelastic material models was then verified by performing single-element uniaxial tension tests.

2.3. Boundary and loading conditions

The deployment of the angioplasty balloon models was simulated through the application of a uniform pressure load upon the inner surface of the balloon membrane. This pressure load was applied over a first load step and then reduced to −0.01 MPa over a second load step to allow for stent/artery recoil. In the free-deployment analyses, a pressure load of 2 MPa was employed to allow for comparison with the manufacturer's compliance data. In the second set of analyses, a pressure load of 1.15 MPa was employed to ensure that the stent was deployed to its nominal diameter of 3 mm. For balloons A and B, the extremities of the balloon membrane were constrained in the longitudinal direction. As a result, the balloon membrane was constrained at its extremities but free to move in both the radial and circumferential directions. For balloon C, the balloon membrane was attached to the catheter and the nodes located at the extremities of the guide wire were fully constrained. As a

Table I. Hyperelastic material constants used to describe the mechanical behaviour of the individual layers of the coronary artery and the atherosclerotic plaque.

Constant	Intima	Media	Adventitia	Plaque
μ_1	−5.70 MPa	−1.84 MPa	−1.99 MPa	0.32 MPa
μ_2	3.58 MPa	1.12 MPa	1.20 MPa	—
μ_3	2.17 MPa	0.73 MPa	0.81 MPa	—
α_1	24.43	21.71	24.61	9.25
α_2	25.00	22.00	25.00	—
α_3	23.24	21.20	23.90	—
D_1	0.85	4.11	3.92	0.13
D_2	0	0	0	—
D_3	0	0	0	—

result, the catheter was free to move in both the radial and circumferential directions during the inflation of the angioplasty balloon. Nodes located at the mid-section of the stent and at the extremities of the artery were also constrained in both the circumferential and longitudinal directions.

2.4. Numerical aspects

All finite element analyses were completed using four compute nodes of an SGI Altix ICE 8200EX cluster, which is administered and maintained by the Irish Centre for High-End Computing. Each compute node consists of two Xeon E5650 hex-core processors and 24 gigabytes of RAM. As the procedures under investigation are highly nonlinear and involve multiple contacting surfaces, the ABAQUS/Explicit solver was employed to perform the analyses. During the analyses, contact between each of the various components was modelled using the general contact algorithm. Friction was also included in the analyses through the specification of a Coulomb friction model, and a static friction coefficient of 0.2 was assumed for each set of contact pairs based on data reported in the literature [44]. As inertia is assumed to have a negligible role in the procedures under investigation, a quasi-static approach was adopted. According to the ABAQUS v6.11 documentation, an explicit analysis may be considered quasi-static so long as the kinetic energy of deforming components does not exceed 5% of their internal energy throughout the majority of the solution. This requirement was met by specifying a solution time of three seconds in each of the analyses.

3. RESULTS AND DISCUSSION

In each of the analyses, the deployment of the stent was characterised by a rapid initial expansion that commenced at the extremities of the stent. This phenomenon, which is commonly referred to as dog-boning, is caused by the over-expansion of the angioplasty balloon at the extremities of the stent and is well documented in the literature [37]. This rapid expansion progressed until the stent achieved a uniform cylindrical configuration, and dog-boning was no longer apparent. From this point onward, any further increase in inflation pressure resulted in only a slight increase in stent diameter. This highly compliant response is consistent with that reported from experimental studies of coronary stent deployment with a semi-compliant angioplasty balloon [37]. In terms of computational expense, 2.9, 3.5 and 4.3 CPU hours and 14.7, 15.6 and 16.9 CPU hours were required for the free-deployment and artery-deployment analyses with balloons A, B and C, respectively.

3.1. Free-deployment results

The configuration of the stent and the angioplasty balloon at various stages during the free-deployment analyses is shown in Figure 3. During its deployment, the diameter of the stent varies quite significantly along both its length and circumference. As such, an average stent diameter was determined at each time step. To calculate this average diameter, the radius at the individual crowns was measured at each time step. The crowns are the curved sections of the stent struts that act as
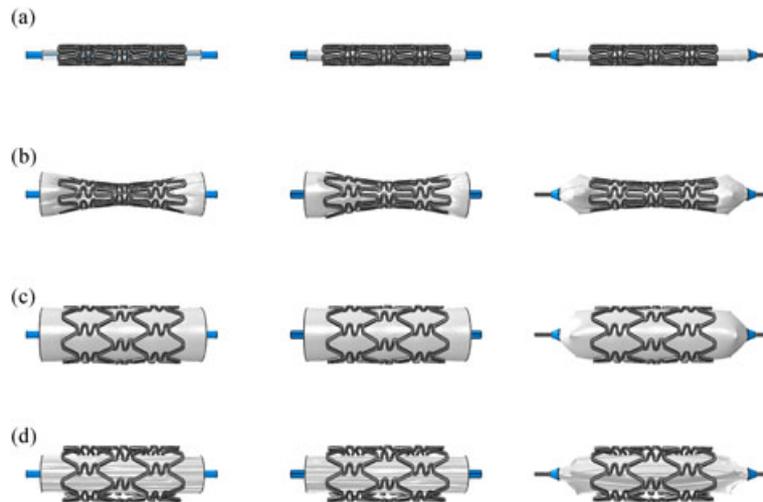
Figure 3. Configuration of the stent (a) prior to loading, (b) during loading, (c) at maximum loading and (d) at unloading of (left) balloon A, (middle) balloon B and (right) balloon C during the free-deployment analyses.
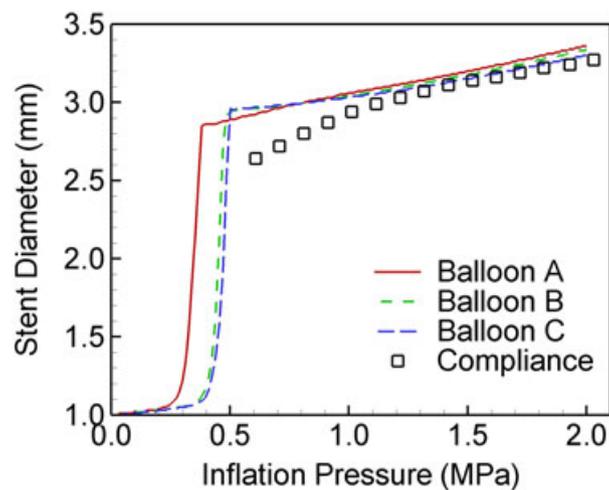

Figure 4. Pressure–diameter response of the stent during the free-deployment analyses compared with manufacturer's compliance data for the BX-Velocity stent.

hinges during its deployment. These values were then averaged and used to calculate the average diameter of the stent at each time step. As shown in Figure 4, the pressure–diameter response of the stent was in good agreement with the manufacturer's compliance data for each of the angioplasty balloon models. Comparing the pressure–diameter results, however, it is clear that the folded configuration of the balloon membrane had a significant influence on the pressure–diameter response of the stent. Specifically, the stent achieved a cylindrical configuration at a lower inflation pressure with balloon A (0.38 MPa) than with either balloon B (0.47 MPa) or balloon C (0.50 MPa). As a result, the stent achieved a greater diameter at unloading of balloon A (3.29 mm) than with either balloon B (3.27 mm) or balloon C (3.22 mm). As the deployment of the stent was in good agreement for balloons B and C, the attachment of the balloon membrane to the catheter did not have a significant influence on the pressure–diameter response of the stent.

To determine the influence of angioplasty balloon configuration on the free-deployment characteristics of the stent, the predicted radial recoil and foreshortening of the stent was measured at unloading of the angioplasty balloon models. Radial recoil, defined as the percentage difference in stent diameter at maximum loading and unloading of the angioplasty balloon, was predicted at 2.54%, 2.53% and 2.55% for balloons A, B and C, respectively. Foreshortening, defined as the percentage difference in stent length prior to loading and at unloading of the angioplasty balloon, was predicted at 8.13%, 8.26% and 6.33% for balloons A, B and C, respectively. Although no significant difference was observed between the predicted rates of radial recoil for each of the angioplasty balloon models, the foreshortening observed at unloading of balloon C was 1.80% lower than that observed at unloading of balloon A and 1.93% lower than that observed at unloading of balloon B. This reduction in foreshortening was attributed to the attachment of the balloon membrane to the catheter, which was neglected for both balloons A and B.

To further investigate the influence of angioplasty balloon configuration on the free-deployment characteristics of the stent, dog-boning was measured throughout each of the analyses. Dog-boning, defined as the percentage difference in diameter at the proximal extremity and mid-section of the stent, reached maximum values of 49.4%, 47.5% and 30.9% for balloons A, B and C, respectively. Comparing the dog-boning results, shown in Figure 5, it is clear that the folded configuration of the balloon membrane had a significant influence on the transient behaviour of the stent. Specifically, maximum dog-boning was observed at a lower inflation pressure with balloon A (0.33 MPa) than with either balloon B (0.44 MPa) or balloon C (0.45 MPa). Furthermore, as the maximum dog-boning observed for balloon B was 35% higher than that observed with balloon C, the attachment of the balloon membrane to the catheter also had a significant influence on the transient behaviour of the stent.

As shown in Figure 6, a similar distribution of equivalent stress was predicted in the stent at unloading of the angioplasty balloon models. In each of the analyses, peak stresses were concentrated in the curved crown segments of the stent that act as hinges during its deployment and undergo significant plastic deformation. As shown in Table II, the peak stress predicted in the stent at unloading of balloon A was 0.18% higher than that observed at unloading of balloon A and 0.84% lower than that observed at unloading of balloon C. The volume-averaged stress predicted in the stent at unloading of balloon A, however, was 4.91% higher than that observed at unloading of balloon B and 7.22% higher than that observed at unloading of balloon C. This difference in volume-averaged stress was attributed to the fact that the stent achieved a greater diameter at unloading of balloon A than at unloading of either balloons B or C. These results suggest that angioplasty balloon configuration had a significant influence on the magnitude of stress predicted in the stent.
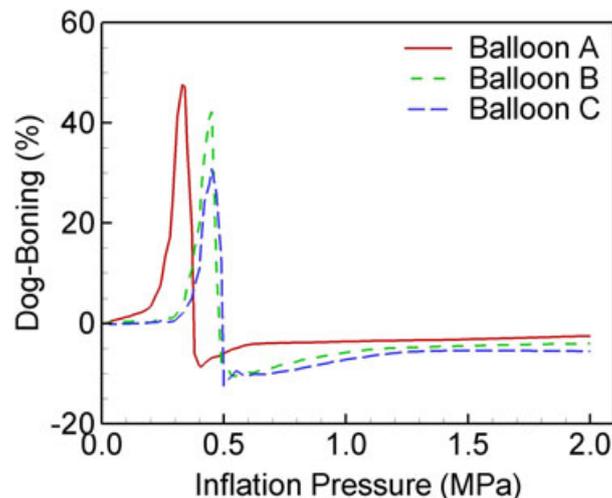

Figure 5. Dog-boning profiles for the stent during the free-deployment analyses.
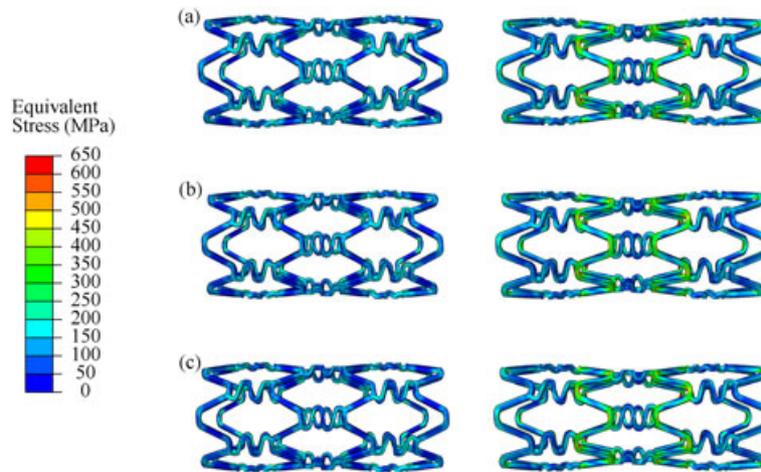
Figure 6. Equivalent stress distribution in the stent at unloading of (a) balloon A, (b) balloon B and (c) balloon C in (left) the free-deployment analyses and (right) the artery-deployment analyses.

Table II. Peak and volume-averaged equivalent stress predicted within the stent at unloading of balloons A, B and C in both the free-deployment and artery-deployment analyses.

Balloon	Peak stress (MPa)	Difference (%)	Volume-averaged stress (MPa)	Difference (%)
Free-deployment analyses				
A	341.43	—	104.24	—
B	340.82	−0.18	99.12	−4.91
C	344.30	+0.84	96.71	−7.22
Artery-deployment analyses				
A	641.53	—	155.58	—
B	640.80	−0.11	151.39	−2.69
C	637.04	−0.70	149.87	−3.67

Note: All differences are taken with respect to balloon A.

3.2. Artery-deployment results

The configuration of the angioplasty balloon, stent and coronary artery during the artery-deployment analyses is shown in Figure 7, and the pressure–diameter response of the stent for each of the angioplasty balloon models is shown in Figure 8. Comparing the pressure–diameter results, it is clear that the folded configuration of the balloon membrane had a significant influence on the pressure–diameter response of the stent. Specifically, the stent achieved a cylindrical configuration at a lower inflation pressure with balloon A (0.32 MPa) than with either balloon B (0.42 MPa) or balloon C (0.44 MPa). As a result, the stent achieved a greater diameter at unloading of balloon A (2.87 mm) than with either balloon B (2.86 mm) or balloon C (2.84 mm). As the deployment of the stent was in good agreement for balloons B and C, the attachment of the balloon membrane to the catheter did not have a significant influence on the pressure–diameter response of the stent.

At unloading of the angioplasty balloon models, radial recoil was predicted at 4.67%, 4.36% and 4.39% for balloons A, B and C, respectively. Compared with the results from the free-deployment analyses, the increase in rates of radial recoil was attributed to the elastic recoil of the artery. Similarly, foreshortening was predicted at 4.88%, 4.75% and 4.25% for balloons A, B and C, respectively. Compared with the results from the free-deployment analyses, the decrease in rates of foreshortening was attributed to the development of frictional forces between the stent and the
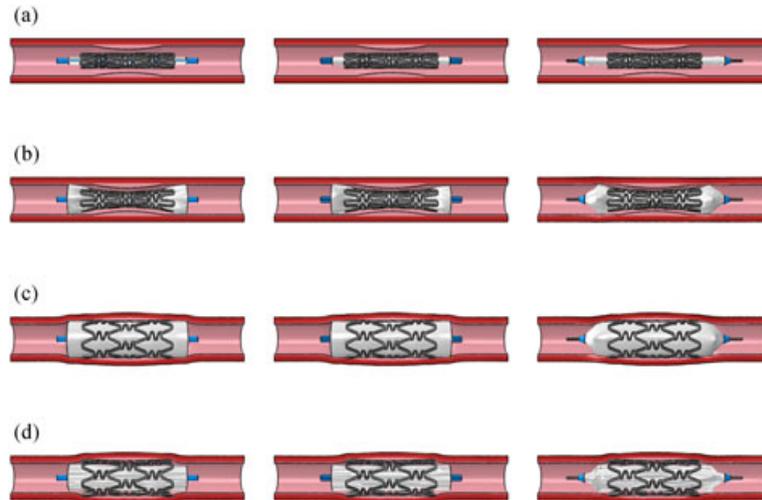
Figure 7. Configuration of the stent/artery (a) prior to loading, (b) during loading, (c) at maximum loading and (d) at unloading of (left) balloon A, (middle) balloon B and (right) balloon C during the artery deployment analyses.
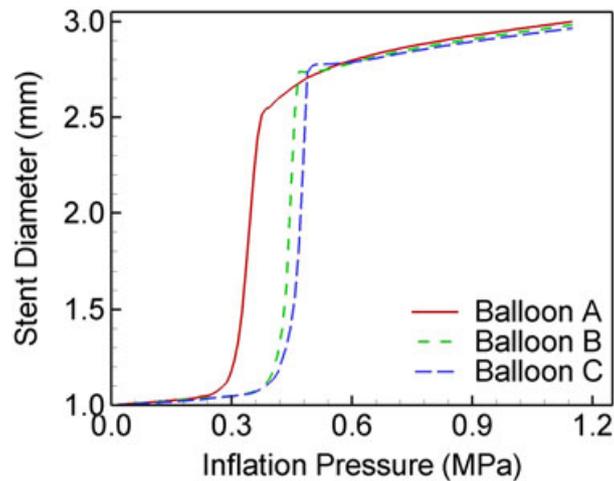

Figure 8. Pressure–diameter response of the stent during the artery-deployment analyses.

artery. Dog-boning reached maximum values of 48.0%, 46.4% and 28.0% for balloons A, B and C, respectively. Again, comparing the dog-boning results, shown in Figure 9, it is clear that the folded configuration of the balloon membrane had a significant influence on the transient behaviour of the stent. Specifically, the maximum dog-boning of the stent was observed at a lower inflation pressure with balloon A (0.31 MPa) than with either balloon B (0.40 MPa) or balloon C (0.42 MPa). As the maximum dog-boning of the stent was 40% higher at unloading of balloon B than at unloading of balloon C, the attachment of the balloon membrane to the catheter also had a significant influence on the transient behaviour of the stent.

As shown in Figure 6, a similar distribution of equivalent stress was predicted within the stent at unloading of each of the angioplasty balloon models. Again, in each of the analyses, peak stresses were concentrated in the curved crown segments of the stent, particularly in the mid-section of the stent where the severity of the plaque was greatest. As shown in Table II, the peak stress predicted
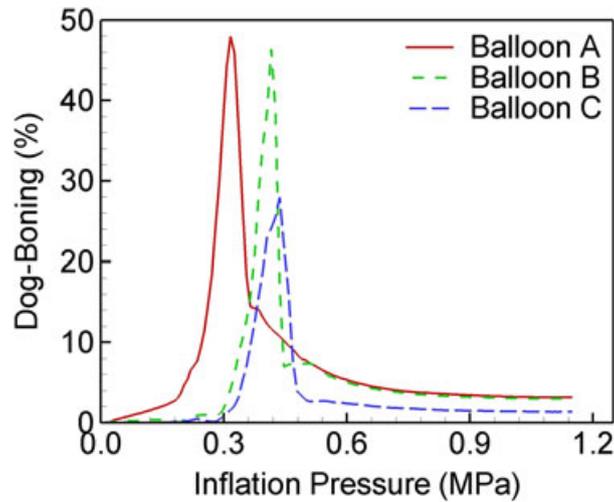
Figure 9. Dog-boning profiles for the stent during the artery-deployment analyses.
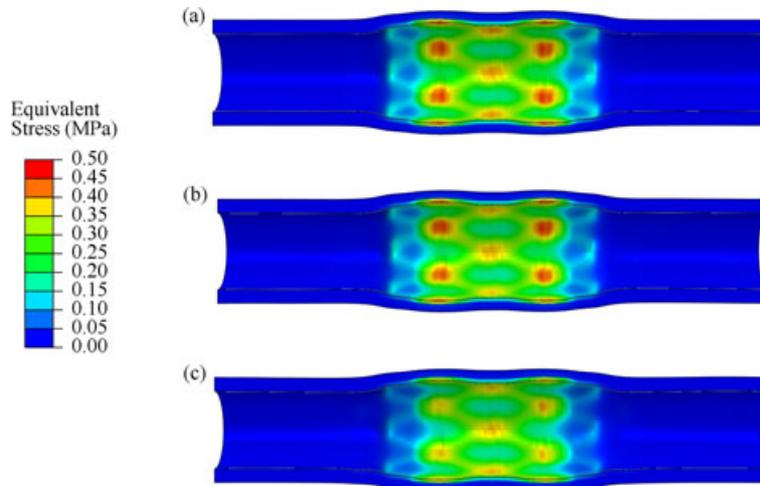

Figure 10. Equivalent stress distribution in the coronary artery at unloading of (a) balloon A, (b) balloon B and (c) balloon C in the artery-deployment analyses.

in the stent at unloading of balloon A was 0.11% higher than that observed at unloading of balloon B and 0.70% higher than that observed at unloading of balloon C. The volume-averaged stress predicted in the stent at unloading of balloon A, however, was 2.69% higher than that observed at unloading of balloon B and 3.67% higher than that observed at unloading of balloon C. As in the free-deployment analyses, the difference in volume-averaged stress was attributed to the fact that the stent achieved a greater diameter at unloading of balloon A than at unloading of either balloons B or C. Again, these results suggest that angioplasty balloon configuration had a marginal influence on the magnitude of stress predicted within the stent.

As shown in Figure 10, a similar distribution of equivalent stress was predicted within the individual layers of the artery at unloading of each of the angioplasty balloon models. In each of the analyses, peak stresses were concentrated in the intimal layer of the artery, particularly in the mid-section of the artery where the severity of the plaque was greatest. As shown in Table III, the peak stresses predicted in the individual layers of the artery at unloading of balloon A were up to 1.7%

Table III. Peak and volume-averaged equivalent stress predicted within the individual layers of the artery at unloading of balloons A, B and C in the artery-deployment analyses.

Balloon	Peak stress (MPa)	Difference (%)	Volume-averaged stress (MPa)	Difference (%)
Intima				
A	0.4988	—	0.1232	—
B	0.4975	−0.26%	0.1184	−3.90%
C	0.4519	−9.40%	0.1092	−11.36%
Media				
A	0.0342	—	0.0109	—
B	0.0336	−1.75%	0.0106	−2.75%
C	0.0313	−8.48%	0.0101	−7.34%
Adventitia				
A	0.0152	—	0.0060	—
B	0.0152	0.00%	0.0059	−1.67%
C	0.0149	−1.97%	0.0056	−6.67%

Note: All differences are taken with respect to balloon A.

higher than those observed at unloading of balloon B and up to 9.4% higher than those observed at unloading of balloon C. Similarly, the volume-averaged stresses predicted in the individual layers of the artery at unloading of balloon A were up to 3.9% higher than those observed at unloading of balloon B and up to 11.4% higher than those observed at unloading of balloon C. Again, this was attributed to the fact that the stent achieved a greater diameter at unloading with balloon A than at unloading of either balloons B or C. These results suggest that angioplasty balloon configuration had a significant influence on the magnitude of stress predicted within the artery.

3.3. Limitations

The analyses reported in this study suffer from a number of sources of limitation, mainly due to the geometric and material models that were employed. The geometry of the stent was generated based on a limited number of dimensions, which are reported in the literature, and as such, it represents merely an approximation of the actual BX-Velocity stent. In recent studies, accurate finite element models of various coronary stents have been generated using micro-CT images of the devices in their crimped configuration [43]. Because of the comparative nature of this study, however, this limitation should not have an adverse impact on the results of the analyses. Despite this limitation, for example, the pressure–diameter response of the stent following the free-deployment analyses was found to be in good agreement with the manufacturer's compliance data. Furthermore, the predicted rates of both radial recoil and foreshortening were similar to values reported in the literature [52, 58].

With regard to the coronary artery, the geometry proposed in this study is heavily idealised and a realistic geometry derived from patient-specific images would be more in line with current state-of-the-art research. Because of the comparative nature of this study, however, the geometrical configuration of the artery is arbitrary and the use of an idealised model should not have a major influence on the conclusions. Additionally, the mechanical behaviour of the artery was described using isotropic material models based on properties derived from circumferentially orientated samples of human arterial tissue. In reality, however, arterial tissue exhibits an anisotropic response in the circumferential and longitudinal directions [55]. Although limiting, the isotropic description of the artery is plausible, however, as the dominant arterial response during stent deployment is in the circumferential direction. Finally, when subject to non-physiological loading, damage to the arterial tissue can elicit an inelastic mechanical response within the artery [59]. This inelastic response may have a significant influence on the behaviour of the artery during coronary stent deployment.

4. CONCLUSION

In this study, the influence of the folded configuration of the balloon membrane and its attachment to the catheter on both the free-deployment of a stent and its impact on the mechanical environment of the coronary artery have been investigated for the first time. Both the free-deployment of the stent and its deployment within an idealised model of a coronary artery was investigated using (a) an idealised non-folded model, (b) an idealised folded model and (c) a state-of-the-art folded model of a semi-compliant angioplasty balloon. On the basis of the results of this study, it is clear that angioplasty balloon configuration has very little influence on the deployed configuration of the stent. This is evident from the deformed configuration of the stent and the rates of radial recoil and foreshortening predicted in each of the analyses. The configuration of the angioplasty balloon does, however, have a significant influence on the transient behaviour of the stent and the magnitude of stress within both the stent and the artery. This is evident from both the pressure–diameter response and dog-boning profile of the stent and from the magnitude of stresses predicted in each of the analyses.

Because of the reduction in computational cost, it is recommended that an idealised angioplasty balloon model is employed in future studies in which the transient behaviour of the stent and the magnitude of stresses are not of critical importance. In the initial stages of stent design, for example, several analyses may be required to optimise the geometry of the stent. Here, both the folded configuration of the balloon membrane and its attachment to the catheter should be neglected. In future studies in which the transient behaviour of the stent and the magnitude and the distribution of stresses are of critical importance, however, it is recommended that a realistic angioplasty balloon model is considered. In the latter stages of stent design, for example, it may be important to investigate the transient behaviour of the stent and its impact upon the mechanical environment of the coronary artery. Here, the folded configuration of the balloon membrane and its attachment to the catheter should be included. These recommendations should aid future research in this area.

REFERENCES

1. Roger V, Go A, Lloyd-Jones D, Adams R, Berry J, Brown T, Carnethon M, Dai S, de Simone G, Ford E, Fox C, Fullerton H, Gillespie C, Greenlund K, Hailpern S, Heit J, Ho P, Howard V, Kissela B, Kittner S, Lackland D, Lichtman J, Lisabeth L, Makuc D, Marcus G, Marelli A, Matchar D, McDermott M, Meigs J, Moy C, Mozaffarian D, Mussolino M, Nichol G, Paynter N, Rosamond W, Sorlie P, Stafford R, Turan T, Turner M, Wong N, Wylie-Rosett J. Heart disease and stroke statistics 2011 update: A Report from the American Heart Association. *Circulation* 2011; **123**:e18–e209.
2. Fischman D, Leon M, Baim D, Schatz R, Savage M, Penn I, Detre K, Veltri L, Ricci D, Nobuyoshi M, Cleman M, Heuser R, Almond D, Teirstein P, Fish R, Colombo A, Brinker J, Moses J, Shaknovich A, Hirshfeld J, Bailey S, Ellis S, Rake R, Goldberg S. A randomized comparison of coronary stent placement and balloon angioplasty in the treatment of coronary artery disease. *New England Journal of Medicine* 1994; **331**:496–501.
3. Morice M, Serruys P, Sousa J, Fajadet J, Ban Hayashi E, Perin M, Colombo A, Schuler G, Barragan P, Guagliumi G, Molnar F, Falotico R. A randomized comparison of a sirolimus-eluting stent with a standard stent for coronary revascularization. *New England Journal of Medicine* 2002; **346**:1773–1780.
4. Moses J, Leon M, Popma J, Fitzgerald P, Holmes D, O'Shaughnessy C, Caputo R, Kereiakes D, Williams D, Teirstein P, Jaeger J, Kuntz R. Sirolimus- eluting stents versus standard stents in patients with stenosis in a native coronary artery. *New England Journal of Medicine* 2003; **349**:1315–1323.
5. Serruys P, de Jaegere P, Kiemeneij F, Macaya C, Rutsch W, Heyndrickx G, Emanuelsson H, Marco J, Legrand V, Materne P, Belardi J, Sigwart U, Colombo A, Goy J, van den Heuvel P, Delcan J, Morel M. A comparison of balloon- expandable-stent implantation with balloon angioplasty in patients with coronary artery disease. *New England Journal of Medicine* 1994; **331**:489–495.
6. Stone G, Ellis S, Cox D, Hermiller J, O'Shaughnessy C, Mann J, Turco M, Caputo R, Bergin P, Greenberg J, Popma J, Russell M. A polymer-based, paclitaxel-eluting stent in patients with coronary artery disease. *New England Journal of Medicine* 2004; **350**:221–231.

7. Mitra A, Agrawal D. In stent restenosis: bane of the stent era. *Journal of Clinical Pathology* 2006; **59**:232–239.
8. Farb A, Sangiorgi G, Carter A, Walley V, Edwards W, Schwartz R, Virmani R. Pathology of acute and chronic coronary stenting in humans. *Circulation* 1999; **99**:44–52.
9. Virmani R, Farb A. Pathology of in-stent restenosis. *Current Opinion in Lipidology* 1999; **10**:499–506.
10. Schwartz R, Huber K, Murphy J, Edwards W, Camrud A, Vlietstra R, Holmes D. Restenosis and the proportional neointimal response to coronary artery injury: Results in a porcine model. *Journal of the American College of Cardiology* 1992; **19**:267–274.
11. Wentzel J, Krams R, Schuurbiers J, Oomen J, Kloet J, van der Giessen W, Serruys P, Slager C. Relationship between neointimal thickness and shear stress after wallstent implantation in human coronary arteries. *Circulation* 2001; **103**:1740–1745.
12. Hehrlein C, Zimmermann M, Metz J, Ensinger W, Kubler W. Influence of surface texture and charge on the biocompatibility of endovascular stents. *Coronary Artery Disease* 1995; **6**:581–586.
13. Martin D, Boyle F. Drug-eluting stents for coronary artery disease: A review. *Medical Engineering and Physics* 2011; **33**:148–163.
14. Balossino R, Gervaso F, Migliavacca F, Dubini G. Effects of different stent designs on local hemodynamics in stented arteries. *Journal of Biomechanics* 2008; **41**:1053–1061.
15. Dehlaghi V, Shadpoor M, Najarian S. Analysis of wall shear stress in stented coronary artery using 3D computational fluid dynamics modeling. *Journal of Materials Processing Technology* 2008; **197**:174–181.
16. Gastaldi D, Sassi V, Petrini L, Vedani M, Trasatti S, Migliavacca F. Continuum damage model for bioresorbable magnesium alloy devices: Application to coronary stents. *Journal of the Mechanical Behavior of Biomedical Materials* 2011; **4**:352–365.
17. Grogan J, O'Brien B, Leen S, McHugh P. A corrosion model for bioabsorbable metallic stents. *Acta Biomaterialia* 2011; **7**:3523–3533.
18. LaDisa J, Guler I, Olson L, Hettrick D, Kersten J, Warltier D, Pagel P. Three-dimensional computational fluid dynamics modeling of alterations in coronary wall shear stress produced by stent implantation. *Annals of Biomedical Engineering* 2003; **31**:972–980.
19. LaDisa J, Olson L, Guler I, Hettrick D, Audi S, Kersten J, Warltier D, Pagel P. Stent design properties and deployment ratio influence indexes of wall shear stress: A three-dimensional computational fluid dynamics investigation within a normal artery. *Journal of Applied Physiology* 2004; **97**:424–430.
20. LaDisa J, Olson L, Guler I, Hettrick D, Kersten J, Warltier D, Pagel P. Circumferential vascular deformation after stent implantation alters wall shear stress evaluated with time-dependent 3D computational fluid dynamics models. *Journal of Applied Physiology* 2005; **98**:947–957.
21. Mejia J, Ruzzeh B, Mongrain R, Leask R, Bertrand O. Evaluation of the effect of stent strut profile on shear stress distribution using statistical moments. *Biomedical Engineering Online* 2009; **8**:8–8.
22. Murphy J, Boyle F. A numerical methodology to fully elucidate the altered wall shear stress in a stented coronary artery. *Cardiovascular Engineering and Technology* 2010; **1**:256–268.
23. Murphy J, Boyle F. A full-range, multi-variable, CFD-based methodology to identify abnormal near-wall hemodynamics in a stented coronary artery. *Biorheology* 2010; **47**:117–132.
24. Vairo G, Cioffi M, Cottone R, Dubini G, Migliavacca F. Drug release from coronary eluting stents: A multidomain approach. *Journal of Biomechanics* 2010; **43**:1580–1589.
25. Wu W, Gastaldi D, Yang K, Tan L, Petrini L, Migliavacca F. Finite element analyses for design evaluation of biodegradable magnesium alloy stents in arterial vessels. *Materials Science and Engineering: B* 2011; **176**:1733–1740.
26. Zunino P, D'Angelo C, Petrini L, Vergara C, Capelli C, Migliavacca F. Numerical simulation of drug eluting coronary stents: Mechanics, fluid dynamics and drug release. *Computer Methods in Applied Mechanics and Engineering* 2009; **198**:3633–3644.
27. Auricchio F, Di Loreto M, Sacco E. Finite-element analysis of a stenotic artery revascularization through a stent insertion. *Computer Methods in Biomechanics and Biomedical Engineering* 2001; **4**:249–263.
28. Capelli C, Gervaso F, Petrini L, Dubini G, Migliavacca F. Assessment of tissue prolapse after balloon-expandable stenting: Influence of stent cell geometry. *Medical Engineering and Physics* 2009; **31**:441–447.
29. David Chua S, Mac Donald B, Hashmi M. Finite-element simulation of stent expansion. *Journal of Materials Processing Technology* 2002; **120**:335–340.
30. David Chua S, Mac Donald B, Hashmi M. Finite element simulation of stent and balloon interaction. *Journal of Materials Processing Technology* 2003; **143–144**:591–597.
31. David Chua S, Mac Donald B, Hashmi M. Finite element simulation of slotted tube (stent) with the presence of plaque and artery by balloon expansion. *Journal of Materials Processing Technology* 2004; **155–156**:1772–1779.
32. De Beule M, Mortier P, Carlier S, Verhegghe B, Van Impe R, Verdonck P. Realistic finite element-based stent design: The impact of balloon folding. *Journal of Biomechanics* 2008; **41**:383–389.
33. Dumoulin C, Cochelin B. Mechanical behaviour modelling of balloon- expandable stents. *Journal of Biomechanics* 2000; **33**:1461–1470.
34. Early M, Kelly D. The role of vessel geometry and material properties on the mechanics of stenting in the coronary and peripheral arteries. *Proceedings of the Institution of Mechanical Engineers, Part H* 2010; **224**:465–476.
35. Etave F, Finet G, Boivin M, Boyer J, Rioufol G, Thollet G. Mechanical properties of coronary stents determined by using finite element analysis. *Journal of Biomechanics* 2001; **34**:1065–1075.

36. Gervaso F, Capelli C, Petrini L, Lattanzio S, Di Virgilio L, Migliavacca F. On the effects of different strategies in modelling balloon-expandable stenting by means of finite element method. *Journal of Biomechanics* 2008; **41**:1206–1212.
37. Kiousis D, Wulff A, Holzapfel G. Experimental studies and numerical analysis of the inflation and interaction of vascular balloon catheter-stent systems. *Annals of Biomedical Engineering* 2009; **37**:315–30.
38. Lally C, Dolan F, Prendergast P. Cardiovascular stent design and vessel stresses: A finite element analysis. *Journal of Biomechanics* 2005; **38**:1574–1581.
39. Liang D, Yang D, Qi M, Wang W. Finite element analysis of the implantation of a balloon-expandable stent in a stenosed artery. *International Journal of Cardiology* 2005; **104**:314–318.
40. McGarry J, O'Donnell B, McHugh P, McGarry J. Analysis of the mechanical performance of a cardiovascular stent design based on micromechanical modelling. *Computational Materials Science* 2004; **31**:421–438.
41. Migliavacca F, Petrini L, Colombo M, Auricchio F, Pietrabissa R. Mechanical behavior of coronary stents investigated through the finite element method. *Journal of Biomechanics* 2002; **35**:803–811.
42. Migliavacca F, Petrini L, Montanari V, Quagliana I, Auricchio F, Dubini G. A predictive study of the mechanical behaviour of coronary stents by computer modelling. *Medical Engineering and Physics* 2005; **27**:13–18.
43. Mortier P, De Beule M, Van Loo D, Verhegghe B, Verdonck P. Finite element analysis of side branch access during bifurcation stenting. *Medical Engineering and Physics* 2009; **31**:434–440.
44. Mortier P, Holzapfel G, De Beule M, Van Loo D, Taeymans Y, Segers P, Verdonck P, Verhegghe B. A novel simulation strategy for stent insertion and deployment in curved coronary bifurcations: Comparison of three drug-eluting stents. *Annals of Biomedical Engineering* 2010; **38**:88–99.
45. Pant S, Limbert G, Curzen NP, Bressloff NW. Multiobjective design optimisation of coronary stents. *Biomaterials* 2011; **32**:7755–7773.
46. Pericevic I, Lally C, Toner D, Kelly D. The influence of plaque composition on underlying arterial wall stress during stent expansion: The case for lesion-specific stents. *Medical Engineering and Physics* 2009; **31**:428–433.
47. Petrini L, Migliavacca F, Auricchio F, Dubini G. Numerical investigation of the intravascular coronary stent flexibility. *Journal of Biomechanics* 2004; **37**:495–501.
48. Tan L, Webb D, Kormi K, Al-Hassani S. A method for investigating the mechanical properties of intracoronary stents using finite element numerical simulation. *International Journal of Cardiology* 2001; **78**:51–67.
49. Wang W, Liang D, Yang D, Qi M. Analysis of the transient expansion behavior and design optimization of coronary stents by finite element method. *Journal of Biomechanics* 2006; **39**:21–32.
50. Zahedmanesh H, John Kelly D, Lally C. Simulation of a balloon expandable stent in a realistic coronary artery: Determination of the optimum modelling strategy. *Journal of Biomechanics* 2011; **43**:2126–2132.
51. Martin D, Boyle FJ. Computational structural modelling of coronary stent deployment: A review. *Computer Methods in Biomechanics and Biomedical Engineering* 2011; **14**:331–348.
52. Serruys P, Rensing B. *Handbook of Coronary Stents*. Dunitz Ltd.: London, 2005.
53. Brauer H, Stolpmann J, Hallmann H, Erbel R, Fischer A. Measurement and numerical simulation of the dilatation behaviour of coronary stents. *Materialwissenschaft und Werkstofftechnik* 2000; **30**:876–885.
54. Laroche D, Delorme S, Anderson T, DiRaddo R. Computer prediction of friction in balloon angioplasty and stent implantation. In *Biomedical Simulation*, Harders M, Sze'kely G (eds). Springer, 2006; 1–8.
55. Holzapfel G, Sommer G, Gasser C, Regitnig P. Determination of layer- specific mechanical properties of human coronary arteries with nonatherosclerotic intimal thickening and related constitutive modeling. *American Journal of Physiology-Heart and Circulatory Physiology* 2005; **289**:H2048–H2058.
56. Poncin P, Proft J. Stent tubing: Understanding the desired attributes. *Medical Device Materials: Proceedings from the Materials & Processes for Medical Devices Conference 2003, 8–10, September 2003*, Anaheim, California, 2004; 253.
57. Loree H, Grodzinsky A, Park S, Gibson L, Lee R. Static circumferential tangential modulus of human atherosclerotic tissue. *Journal of Biomechanics* 1994; **27**:195–204.
58. Colombo A, Stankovic G, Moses J. Selection of coronary stents. *Journal of the American College of Cardiology* 2002; **40**:1021–1033.
59. Pena E, Alastrue V, Laborda A, Martinez M, Doblare M. A constitutive formulation of vascular tissue mechanics including viscoelasticity and softening behaviour. *Journal of Biomechanics* 2010; **43**:984–989.